Research Article | Vol. 27, No. 15 | 22 Jul 2019 | OPTICS EXPRESS 21020
Optics EXPRESS

Manipulating dynamical Rabi-splitting with two-color laser pulses

H. AGUENY,[1,*] A. TAOUTIOUI,[2] Y. ADNANI,[3] AND A. MAKHOUTE[2,4]

[1]*Department of Physics and Technology, Allegt. 55, University of Bergen, N-5007 Bergen, Norway*
[2]*Physique du Rayonnement et des Interactions Laser-Matière, Faculté des Sciences. Université Moulay Ismail, B.P. 11201, Zitoune, Meknes, Morocco*
[3]*Ecole Supérieure de Technologie. Université Ibn Tofail P.B 242, Kenitra, Morocco*
[4]*Faculté des Sciences, Université Libre de Bruxelles (ULB), Boulevard du Triomphe, 1050 Brussels, Belgium*
[*]*hicham.agueny@uib.no*

Abstract: We theoretically investigate strong-field ionization of hydrogen atoms by orthogonally polarized two-color (OTC) laser pulses consisting of a fundamental field that is resonant with the $1s-2p$ transition and its second harmonic. Numerical simulations are performed by solving the two-dimensional time-dependent Schrödinger equation and recording the photoelectron momentum distribution. In this strong-field resonant ionization, the atom undergoes many Rabi cycles and the electron can be emitted within a completed Rabi-cycle leading to the splitting of the localized momentum distribution. Here, the splitting is attributed to dynamic Rabi-splitting as a result of the dynamic Stark effect.The employed OTC scheme is shown to be efficient for controlling the dynamic Rabi-splitting through the control of quantum-path interferences involved in one-photon and two-photon absorption processes. The control scheme is accomplished by varying the relative ratio intensity and optical phase between the two pulses, and its footprint is mapped in the momentum distribution. This is shown to lead to an asymmetric distribution and suppression of the ionization process. The obtained results suggest the OTC scheme as a tool for coherent control of dynamic Rabi-oscillations via the controlled quantum-path interferences, thus opening new directions towards designing quantum states via the control OTC scheme.

1. Introduction

The dynamics of two atomic levels involved in an atomic transition mediated by a coherent resonant laser pulse leads to novel phenomena manifested by their nonlinearity. Rabi-oscillation is one of such phenomena. The effect is of fundamental interest to modern quantum physics and considered one of the most manifestations of coherent light-matter interactions. Its particularity is related to the ability to form the basis for many applications such as atomic clocks, quantum computing and information processing [1], and quantum control of nano-devices at the electronic level [2, 3].

Over the past decade significant progress in studying Rabi oscillations has been made, and a variety of physical processes belonging to the areas of quantum computing, condensed matter and atomic and molecular physics have been investigated. This has led to new findings related for instance to their real-time observation [4], their ultrafast control [5], their observation in a collection of atoms [6], and even their observation in connection with multiphotonic processes [7, 8]. In the latter process, a direct experimental observation of a Rabi-cycling in the XUV-regime has been reported [7, 8], suggesting thus Rabi process as a new tool for direct coherent control of light-matter interactions. This statement gets support from theoretical studies, where Rabi effect has been investigated in strongly correlated electrons, providing thus new insights into electronic correlations and multiphotonic processes [9–11].

Rabi-oscillations have been mostly studied in connection with the spectral domain (see,

#367546 https://doi.org/10.1364/OE.27.021020
Journal © 2019 Received 15 May 2019; revised 13 Jun 2019; accepted 13 Jun 2019; published 12 Jul 2019

Optics EXPRESS

e.g., [7, 12, 13] and references therein). Their investigation in the two-dimensional (2D) photoelecron momentum distribution will be of particular interest when a second laser pulse is introduced as a control scheme. In this situation, quantum interferences between photoelectron partial waves with opposite-parity, due to the two components of the laser pulses, may emerge in the 2D-photoelectron momentum distribution. The emergence of these interesting coherent effects can be exploited for quantum information processing and computing.

Motivated by general interest of Rabi oscillations as a powerful tool to prepare and manipulate quantum states, we propose in this work a control scheme based on orthogonally polarized two-color (OTC) laser pulses to gain control over the electron dynamics. Introducing this OTC scheme has shown to provide an unprecedented insight into light-induced electronic processes, enabling thus to coherently control their dynamical behavior. For instance, the OTC scheme has been used recently to control temporal double-slit interference [14], to identify the non-adiabatic sub-cycle electron dynamics [15], to disentangle intra-cycle interferences [16] and to control temporal interferences [17]. Controlling the correlated electron dynamics in non-sequential double ionization processes via two-color scheme has also been reported [18, 19], allowing thus to measure the time-delay between the released two-electrons [20]. These phenomena have been recorded in the 2D-photoelectron momentum distribution, offering thus the potential to directly access the ultrafast electron dynamics. To our knowledge, manipulating Rabi-oscillations by means of the OTC control scheme have not been reported previously.

It is the purpose of this paper to investigate the photoelectron momentum distribution to learn about ultrafast electron dynamics using OTC laser pulses. This is achieved by solving the 2D time-dependent Schrödinguer equation (2D-TDSE). Here, the ionization dynamics is mainly induced by the fundamental harmonic field, which is chosen to be resonant with the $1s - 2p$ transition, while its second harmonic is used to control the dynamics. Here, we show that using this OTC scheme offers a new and intriguing degree of control freedom for dynamical Rabi oscillations. The control scheme explores the quantum path interferences between electron wave packet generated by one-photon and two-photon processes in the final momentum state. We show that the emergence of these effects can be manipulated by varying the relative ratio intensity and optical carrier envelope phase of the two pulses.

The paper is organized as follows. In Sec. II, we provide the theoretical basis for the electron dynamics, which is based on the 2D-TDSE. Section III is devoted to the analysis of the 2D-photoelectron momentum distributions and particularly to identify Rabi-oscillations and investigate the possibility of their coherent control by varying the properties of the OTC laser pulses. Finally, conclusions are given in Sec. IV. Atomic units are used in this article unless otherwise indicated.

2. Theoretical background

The dynamics of a hydrogen atom interacting with orthogonally polarized laser fields is governed by the TDSE and expressed in two-dimensional (2D) Cartesian coordinates, which reads

$$\Big[H_0 + V_I(t) - i\frac{\partial}{\partial t}\Big]\psi(\vec{r}, t) = 0, \tag{1}$$

where $\vec{r} = (x, z)$ denotes the vector position of the electron. In the field-free Hamiltonian H_0, we adopt a regularized 2D Coulomb potential [21]

$$H_0 = -\frac{1}{2}\frac{\partial^2}{\partial z^2} - \frac{1}{2}\frac{\partial^2}{\partial x^2} - \frac{1}{\sqrt{x^2 + z^2 + 0.64}}. \tag{2}$$

The time-dependent interaction $V_I(t)$ is treated in the velocity gauge and can be expressed within the dipole interaction as

$$V_I(t) = \vec{p} \cdot \vec{A}(t), \tag{3}$$

Optics EXPRESS

where $\vec{p}$=(p_x,p_z) denotes the vector momentum of the electron and $\vec{A}(t) = (A_x, A_z)$ is the vector potential having the two components, respectively, along x- and z-axes

$$A_x(t) = \sqrt{\eta}\frac{E_0}{\omega} f(t)\sin(2\omega t + \varphi_{CEP}) \quad (4)$$

$$A_z(t) = \frac{E_0}{\omega} f(t)\sin(\omega t) \quad (5)$$

Here, E_0 is the maximum field strength and ω represents the angular frequency of the fundamental harmonic field and its second harmonic frequency is 2ω. The pulse envelope $f(t)$ has a Gaussian-shaped $e^{-4\ln(2)t^2/\tau^2}$ form with $\tau = 2\pi N_c/\omega$ is the full width at half maximum of the field envelope. Here, N_c is the total number of cycles. η and φ_{CEP} represent the relative ratio of the peak intensity (defined as $I_0 = E_0^2$) and the relative carrier envelope phase of the OTC laser pulses. The parameter η determines the role of the second pulse in the OTC scheme [14, 22]. In this work the η is chosen such that the second pulse acts as a control pulse (i.e. $\eta < 1$).

Initially, the system is considered to be in the ground state. The temporal evolution of the wave function $\psi(x, z)$ satisfying the TDSE [cf. Eq. (1)], is solved numerically by combining a split-operator method with a fast Fourier transform algorithm [23]. The numerical integration is carried out on a symmetric grid $[-x, x] \times [-z, z]$ of size $|z| = |x|$=512 a.u. with the spacing grid $\Delta z = \Delta x$ =0.25 a.u., i.e. 4096 grid points along z- and x-axis directions.

During the simulations, the time step is fixed at $\Delta t = 0.05$ a.u., and the convergence is checked by performing additional calculations with twice the size of the box with a smaller time step. We employ an absorber to avoid artificial reflections. This is chosen to span 10% of the grid size in each direction. At the end of the interaction $t = t_f$, where the laser pulses are swished off, we calculate the 2D- photoelectron momentum distribution. This is done by performing the Fourier transform of the spatial ionization wave function ψ_{ioniz} [24, 25]. The latter is obtained using the projection technique [26, 27]. In this technique we consider orthogonal projection operators $\hat{P}$ and $\hat{Q}$, such that

$$\hat{Q} = 1 - \hat{P} = 1 - \sum_i^N |\psi_i\rangle\langle\psi_i|, \quad (6)$$

where $|\psi_i\rangle$ are the eigenvectors of the field-free Hamiltonian H_0 [cf. Eq. (2)]. The spatial ionization wave function ψ_{ioniz} can be written

$$|\psi_{ioniz}\rangle = \hat{Q}|\psi(t_f)\rangle. \quad (7)$$

Substituting Eq. (6) into Eq. (7) we obtain ψ_{ioniz}

$$\psi_{ioniz}(x, z) = \psi(x, z, t_f) - \sum_i \psi_i(x, z) \int\int \psi_i(x', z')\psi(x', z', t_f)dx'dz', \quad (8)$$

where the sum over the important bound states ψ_i, which are obtained using imaginary time propagation, covers the first nine excited states. The convergence of the momentum distribution with respect to the extraction of the excited states is checked, ensuring thus the numerical convergence of our results.

3. Results and discussion

We start our discussion by looking at the strong-field ionization dynamics of the hydrogen atom by employing a single-color laser pulse. The laser pulse is resonant with the $1s - 2p$ transition having the photon energy of ω = 8.58 eV (λ= 144.53 nm) and is linearly polarized along the z-axis. The results stemming from this single-color scheme are shown in Fig. 1 and represent the photoelectron momentum distribution. These are shown for three-peak intensities: 4×

Optics EXPRESS

10^{12}, 6× 10^{13} and 2× 10^{14} W/cm^2. As seen in Fig. 1, the distributions exhibit a rich structure, which manifests by a splitting of the localized momentum distribution that is located around $\sqrt{2(2\omega - I_p \pm \Omega_{Rabi}/2)}$, where I_p is the ionization potential and $\Omega_{Rabi} = E_0\langle 1s \mid z \mid 2p\rangle$ is the Rabi frequency. These features emerge on both polarization directions and exhibit a strong dependence on the pulse intensity.

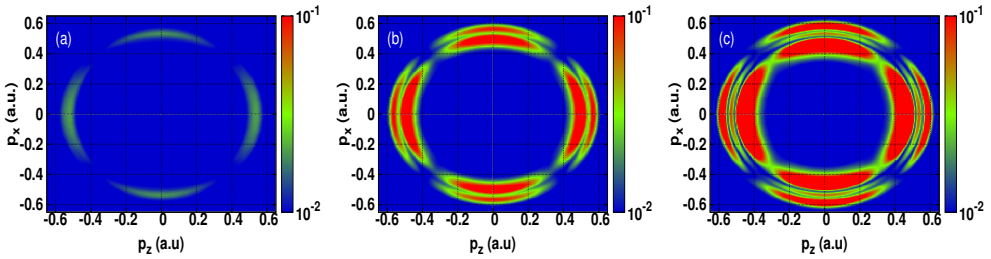

Fig. 1. 2D-photoelectron momentum distributions of the hydrogen atom resulting from a single-color scheme. The results are shown for a fixed photon energy ω = 8.58 eV (λ= 144.53 nm) and for three peak intensities: (a) 4× 10^{12} W/cm^2; (b) 6× 10^{13} W/cm^2; (c) 2× 10^{14} W/cm^2.

In order to provide more insight in the observed splitting, we show in Fig. 2 the amplitude $|\langle\psi(t = 0)|\psi(t)\rangle|$ and phase $\zeta(t)$ of the population of the ground state as a function of time of the pulse. The latter contains information about the dynamic Stark effect [28, 29] and helps to understand the origin of the splitting behavior. The quantities defined above are extracted from the time-dependent wave function $|\psi(t)\rangle$ i.e. $\langle\psi(t = 0)|\psi(t)\rangle = |\langle\psi(t = 0)|\psi(t)\rangle|e^{-i\zeta(t)}$ [30]. Here, we use the same parameters of the laser pulse as in Fig. 1. The peak intensities are 4× 10^{12} (Fig. 2(a)), 6× 10^{13} (Fig. 2(b)) and 2× 10^{14} W/cm^2 (Fig. 2(c)).

At first glance, the population amplitude (black curve) exhibits Rabi oscillations due to the coherent resonant laser pulses and the number of Rabi cycles increases with increasing the peak intensity. Further insights into this oscillatory behavior are provided by the phase $\zeta(t)$ of the amplitude of the ground state. As seen in Fig. 2, the phase (green curve) evolves linearly until it reaches a certain region of the laser pulse (its vector potential is plotted with a blue curve), where the linearity breaks down [cf. Fig. 2(b) and 2(c)]. Here, the phase exhibits abrupt changes of the dressed ground state, resulting in a phase jump. It is found that, in this region, the population of the ground state is depleted. This, however, is not the case at lower intensity [cf. Fig. 2(a)], where the amplitude decays with time. On the other hand, the phase is shown to be constant during the total duration of the pulse with a complete absence of any dynamical aspect. As a result, no splitting emerges as one can see in Fig. 1(a). It turns out that this phase jump is very sensitive to the pulse intensity. By increasing the peak intensity, the phase jump is shown to emerge during the sub-cycle dynamics once at the peak intensity 6× 10^{13} W/cm^2 [cf. Fig. 2(b)] and three-times at 2× 10^{14} W/cm^2 [cf. Fig. 2(c)], thus reflecting the observed splitting in the photoelectron momentum distributions. This becomes clear when the peak intensity is too weak to induce Rabi-oscillations and therefore, no splitting of the localized momentum distribution is emerged.

It is well-known that in the case of a two bound states resonantly coupled by a strong laser pulse, the dressed states repel each other and split in energy. The splitting occurs during the resonant dynamics owing to the induced time-dependent Stark-shift, which follows adiabatically the pulse envelope [31]. The Stark-shift is encoded in the phase, which we refer to as phase jump, and causes the splitting effect that is mapped into the momentum distribution. A similar splitting effect was observed in the spectral domain and discussed in connection with a non-resonant

Optics EXPRESS

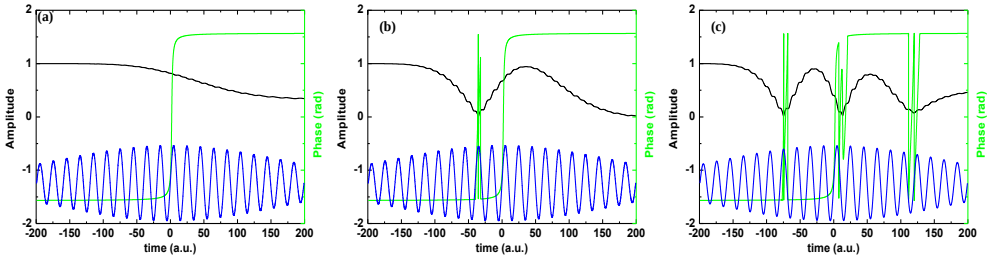

Fig. 2. Amplitude (black curve) and phase (green curve) population of the ground state obtained within a single-color scheme. The results are shown for a fixed photon energy ω = 8.58 eV (λ= 144.53 nm) and for three peak intensities: (a) 4× 10^{12} W/cm^2; (b) 6× 10^{13} W/cm^2; (c) 2× 10^{14} W/cm^2. The amplitude and phase are extracted from the time-dependent wave function: $\langle\psi(t=0)|\psi(t)\rangle = |\langle\psi(t=0)|\psi(t)\rangle|e^{-i\zeta(t)}$ (see text). The blue curve represents the vector potential of the laser pulse.

one-photon ionization. The latter was found to be caused by dynamic Stark effect [32].

Further details about the Rabi-splitting are provided by looking at the temporal evolution of the ionized wave packet. The latter is calculated by projecting out the dressed states, which are obtained at each time of the pulse, from the time-dependent wave function using Eq. (8). The build-up of the Rabi-splitting in time domain is shown in Fig. 3 at the peak intensity 2× 10^{14} W/cm^2. Here, in the beginning of the ionization, only one pronounced peak appears during the rising part of the pulse. The emerging peak is seen to occur at the time of the phase jumping [cf. Fig. 2(c)]. In the falling part of the pulse, the wave packet gets split leading to two pronounced peaks. This splitting is found to occur once again at the time, where the phase jump emerges (around the time 25 a.u.), but unlike in the rising part of the pulse, the phase jump oscillates faster. Further splitting occurs around the time 120 a.u. and is found to evolve periodically in time without any changes. Here we continue propagating the wave packet after the laser pulse is being switched off for an additional 50 a.u. to check the convergence of the observed splitting. The results remain unchanged, ensuring thus their convergence.

At this point, we conclude that the time-dependent phase jump initiates the ionization dynamics leading to the splitting of the ionized wave packet. This splitting is indeed a result of the dynamic Stark effect, which in turn leads to the dynamic Rabi splitting.

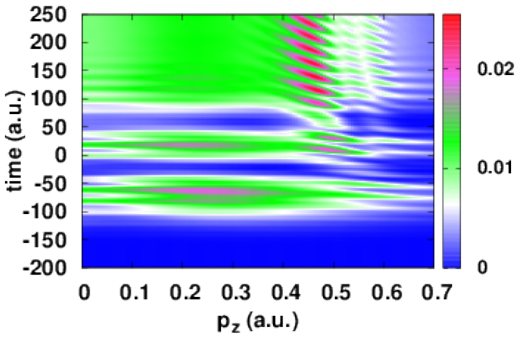

Fig. 3. Temporal evolution of the ionized wave packet in momentum space integrated over the p_x direction. The results are shown at the peak intensity of 2× 10^{14} W/cm^2 and for the photon energy ω = 8.58 eV.

Optics EXPRESS

We now turn to discuss the possibility of controlling this dynamic Rabi-splitting. To this end, we introduce a second laser pulse, where its characteristics are chosen to gain control over Rabi-splitting. Here, we suggest an OTC scheme that comprises a fundamental (λ= 144.53 nm) pulse and its second harmonic ($\lambda/2$= 72.26 nm) and which are linearly polarized, respectively, along the z- and x-axes. In this scheme the fundamental field contributes mainly to the ionization dynamics and is chosen to be resonant with the $1s-2p$ transition (the corresponding photon energy is ω= 8.58 eV), while its second harmonic is employed to control the light-induced resonant ionization and its photon energy is 2ω=17.16 eV. Here, we use the same pulse duration for both laser pulses τ=398.62 a.u. = 9.64 fs. The combined fields are expected to induce interesting coherence effects related to quantum-path interference due to the two components of the OTC scheme, which can be monitored by varying the relative optical pulse phase.

Figure 4 summarizes the results obtained by the OTC scheme and illustrates the role of the streaking field on the Rabi-splitting. Here the peak intensity of the fundamental field is 2×10^{14} W/cm^2 and the relative intensity ratio is η=0.5 (i.e. 1×10^{14} W/cm^2). At the first glance, the momentum distribution in Fig. 4(a) exhibits an asymmetric profile of the Rabi-splitting, and that occurs mainly along the polarization direction of the streaking field. In addition, a suppression of the middle peak is seen to emerge. The asymmetry and the ionization suppression are found to be sensitive to the intensity of the streaking field.

To understand the origin of these features, we perform calculations for the OTC fields separately: We solve the TDSE within a single-color scheme for the fundamental field (i.e. two-photon process), where the obtained ionization wave function is referred to as $\widetilde{\psi}_{\omega}$, and similarly for its second harmonic (i.e. one-photon process), and the obtained ionization wave function is $\widetilde{\psi}_{2\omega}$. A coherent sum of these ionization wave functions (i.e. $|\widetilde{\psi}_{\omega}-\widetilde{\psi}_{2\omega}|^2$) is displayed in Fig. 4(b), and shows the emergence of the asymmetric Rabi-splitting along the polarization direction of the streaking field. Furthermore, the suppression of the middle peak is also reproduced; in agreement with the results stemming from the combined OTC fields [cf. Fig. 4(a)]. This asymmetry and the suppression are however, absent when only the incoherent sum is considered (i.e. $|\widetilde{\psi}_{\omega}|^2+|\widetilde{\psi}_{2\omega}|^2$) [cf. Fig. 4(c)]. Thus, suggesting the interference between electron wave packets generated with the two components of the OTC fields that reach the continuum with the same final momentum to be the origin of these observed features. To be specific, these interference effects result from interferences between d- and s-waves generated by the resonant two-photon process and p-wave generated during the one-photon process. The interplay between these quantum-path interferences and dynamic Rabi-splitting manifests by the observed asymmetric profile of the splitting of the momentum distribution.

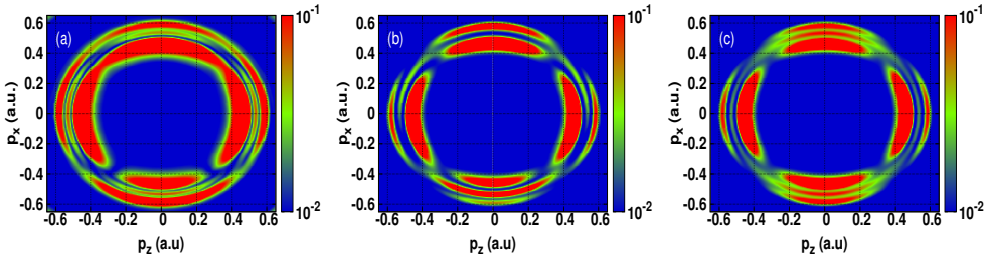

Fig. 4. 2D-photoelectron momentum distributions of the hydrogen atom. The peak intensity is 2×10^{14} W/cm^2, the relative ratio intensity is fixed at $\eta=0.5$ and the relative optical phase is $\varphi_{CEP}=0$. (a) Full OTC scheme; (b) Coherent sum of the ionization wave functions stemming from the individual components of the OTC fields ($|\widetilde{\psi}_{\omega}(p_x,p_z)-\widetilde{\psi}_{2\omega}(p_x,p_z)|^2$) (see Eq. (8)). (c) Incoherent sum $|\widetilde{\psi}_{\omega}(p_x,p_z)|^2+|\widetilde{\psi}_{2\omega}(p_x,p_z)|^2$. Here $\widetilde{\psi}_i(p_x,p_z)$ ($i=\omega,2\omega$) is a Fourier transform of the spatial ionization wave function $\psi_i(x,z)$.

Optics EXPRESS

The dependence of the ionization asymmetry on the intensity of the streaking field is shown in Fig. 5. Here, the momentum distribution is displayed along the polarization of the streaking field by integrating over the momentum p_z. This is shown at the peak intensity of the fundamental field 2×10^{14} W/cm^2 and at three intensities of the streaking field: 5×10^{12} ($\eta = 0.025$), 5×10^{13} ($\eta = 0.25$) and 1×10^{14} W/cm^2 ($\eta = 0.5$). The choice of these intensities is such that the streaking field acts as a control field. For reference, the momentum distribution obtained in the absence of the streaking field is also shown (red thick curve). The results show a strong sensitivity of the asymmetric profile and the splitting effect to the change of the peak intensity. This suggests the streaking field as an efficient control scheme for dynamic Rabi-splitting.

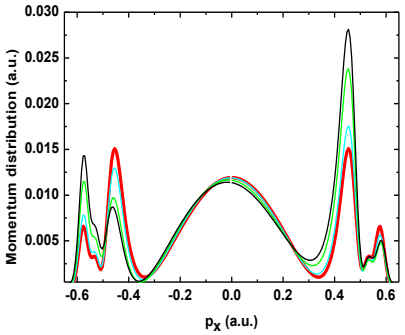

Fig. 5. 1D-photoelectron momentum distributions along the polarization of the streaking field and integrated over the momentum p_z. The peak intensity of the fundamental harmonic field is fixed at 2×10^{14} and the relative ratio intensity is fixed at three values: $\eta = 0.025$ (i.e. 5×10^{12}) (cyan curve), $\eta = 0.25$ (i.e. 5×10^{13}) (green curve), $\eta = 0.5$ (i.e. 1×10^{14} W/cm^2) (black curve). For reference, the distribution obtained in the absence of the streaking field is also shown (red thick curve).

For completeness, we show in the following that Rabi-splitting can be further controlled through the control of quantum-path interferences in the final state. This can be achieved by varying the relative optical phase φ_{CEP}, which influences the final momentum of the electron. Indeed, during the ionization dynamics, electrons are generated with different final momenta depending on the optical phase [33]. This can be understood from the classical equation of motion that describes the final momentum of the electron i.e. $\Delta\vec{p}(t_{ioniz}) = \int_{t_{ioniz}}^{\infty} E(t)dt$, where t_{ioniz} is the ionization time. The final momentum of the electron $\vec{p}_f(t_{ioniz})$ can be read

$$\vec{p}_f(t_{ioniz}) = \vec{p}_i + \Delta\vec{p}(t_{ioniz}) = \vec{p}_i + \vec{A}(t_{ioniz}), \tag{9}$$

where $\vec{p}_i$ is the initial momentum. From this equation, it becomes clear that the change on the final momentum is directly related to the vector potential. Accordingly, by varying the optical phase one can directly control the final momentum and hence get insight into the ionization mechanism (i.e. dynamic Rabi-splitting).

The dependence of the Rabi-splitting on the relative optical phase is shown in Fig. 6. Here, the same laser parameters are used as in Fig. 4(a) and the results are shown for three relative optical phases: $\varphi_{CEP} = \pi/4$, $\pi/2$ and π. Interestingly enough, the asymmetric distribution and also the suppression of the middle peak, are found to be very sensitive to the change of the relative optical phase. This sensitivity, on one side, confirms the origin of the asymmetric ionization as a consequence of quantum-path interference involved in one-photon and two-photon absorption processes and on the other side, reveals once again the role of the streaking field in the OTC scheme as an attractive means of controlling the dynamic Rabi-splitting.

Optics EXPRESS

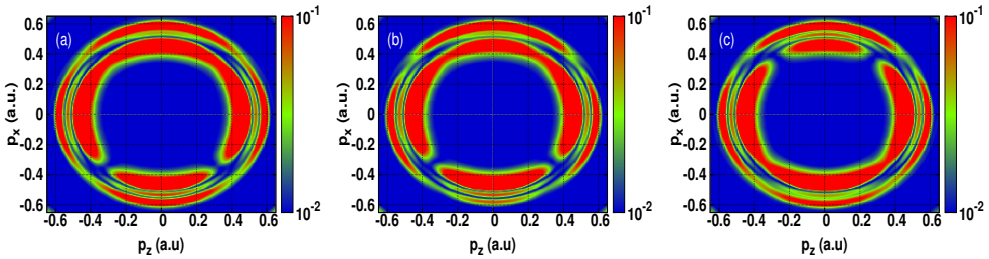

Fig. 6. 2D-photoelectron momentum distributions of hydrogen atoms resulting from the OTC fields at three relative optical phases φ_{CEP}: (a) $\varphi_{CEP} = \pi/4$; (b) $\varphi_{CEP} = \pi/2$; (c) $\varphi_{CEP} = \pi$. The peak intensity is 2×10^{14} W/cm^2 and the relative ratio intensity is fixed at $\eta = 0.5$ (i.e. 1×10^{14} W/cm^2).

4. Conclusions

In conclusion, the light-induced resonant ionization dynamics assisted by a streaking field within the OTC scheme has been theoretically studied by solving the 2D-TDSE. The dynamics has led to the emergence of dynamic Rabi-splitting in the photoelectron momentum distribution accompanied with an asymmetric ionization profile. We have identified the physical mechanism behind the observed asymmetric distribution and the suppression of the ionization and found to result from quantum-path interferences between electron wave packet generated by one-photon and two-photon processes and which reaches the continuum with the same final momentum. Taking advantage of the combined OTC laser fields, we have shown that the Rabi-splitting can be manipulated by varying the relative ratio intensity and optical phase of the two pulses, leading to a substantial asymmetric profile.

Our study provides a comprehensive picture of the crucial role of the OTC scheme to control Rabi-splitting which manifest theme-self in the photoelectron momentum distribution. We believe that the results presented in this work may have direct implications for photoelectron interferometer-based on the OTC scheme to probe the electron dynamics. Furthermore, manipulating Rabi-oscillations by means of the OTC control scheme may open up new directions towards designing quantum states for quantum computing and information processing purposes. The current progress and developments of new light sources make the experimental investigation of the suggested control scheme feasible.

Acknowledgments

The research was supported by UNINETT Sigma2 AS which manages the national infrastructure for computational science in Norway. Numerical calculations were carried out at the Linux cluster Fram (Lenovo NeXtScale nx360).

References

1. M. Saffman, T. G. Walker, and K. Mølmer, "Quantum information with Rydberg atoms," Rev. Mod. Phys. **82**, 2313–2363 (2010).
2. C. Qian, S. Wu, F. Song, K. Peng, X. Xie, J. Yang, S. Xiao, M. J. Steer, I. G. Thayne, C. Tang, Z. Zuo, K. Jin, C. Gu, and X. Xu, "Two-photon Rabi splitting in a coupled system of a nanocavity and exciton complexes," Phys. Rev. Lett. **120**, 213901 (2018).
3. H.-J. Chen, "Auxiliary-cavity-assisted vacuum Rabi splitting of a semiconductor quantum dot in a photonic crystal nanocavity," Photon. Res. **6**, 1171–1176 (2018).
4. P. Vasa, W. Wang, R. Pomraenke, M. Lammers, M. Maiuri, C. Manzoni, G. Cerullo, and C. Lienau, "Real-time observation of ultrafast Rabi oscillations between excitons and plasmons in metal nanostructures with J-aggregates," Nat. Photon. **7**, 128–132 (2013).

Optics EXPRESS

5. L. Dominici, D. Colas, S. Donati, J. P. Restrepo Cuartas, M. De Giorgi, D. Ballarini, G. Guirales, J. C. López Carreño, A. Bramati, G. Gigli, E. del Valle, F. P. Laussy, and D. Sanvitto, "Ultrafast control and Rabi oscillations of polaritons," Phys. Rev. Lett. **113**, 226401 (2014).
6. Y. Dudin, L. Li, F. Bariani, and A. Kuzmich, "Observation of coherent many-body Rabi oscillations," Nat. Phys. **8**, 790–794 (2012).
7. M. Fushitani, C.-N. Liu, A. Matsuda, T. Endo, Y. Toida, M. Nagasono, T. Togashi, M. Yabashi, T. Ishikawa, Y. Hikosaka, T. Morishita, and A. Hishikawa, "Femtosecond two-photon Rabi oscillations in excited He driven by ultrashort intense laser fields," Nat. Photon. **10**, 102–105 (2016).
8. M. Flögel, J. Durá, B. Schütte, M. Ivanov, A. Rouzée, and M. J. J. Vrakking, "Rabi oscillations in extreme ultraviolet ionization of atomic argon," Phys. Rev. A **95**, 021401 (2017).
9. T. Sako, J. Adachi, A. Yagishita, M. Yabashi, T. Tanaka, M. Nagasono, and T. Ishikawa, "Suppression of ionization probability due to Rabi oscillations in the resonance two-photon ionization of He by EUV free-electron lasers," Phys. Rev. A **84**, 053419 (2011).
10. Q. Liao, Y. Zhou, C. Huang, and P. Lu, "Multiphoton Rabi oscillations of correlated electrons in strong-field nonsequential double ionization," New J. Phys. **14**, 013001 (2012).
11. Y. Chen, Y. Zhou, Y. Li, M. Li, P. Lan, and P. Lu, "Rabi oscillation in few-photon double ionization through doubly excited states," Phys. Rev. A **97**, 013428 (2018).
12. M. F. Ciappina, J. A. Pérez-Hernández, A. S. Landsman, T. Zimmermann, M. Lewenstein, L. Roso, and F. Krausz, "Carrier-wave Rabi-Flopping signatures in high-order harmonic generation for alkali atoms," Phys. Rev. Lett. **114**, 143902 (2015).
13. M. G. Girju, K. Hristov, O. Kidun, and D. Bauer, "Nonperturbative resonant strong field ionization of atomic hydrogen," J. Phys. B: At. Mol. Opt. Phys. **40**, 4165–4178 (2007).
14. M. Richter, M. Kunitski, M. Schöffler, T. Jahnke, L. P. H. Schmidt, M. Li, Y. Liu, and R. Dörner, "Streaking temporal double-slit interference by an orthogonal two-color laser field," Phys. Rev. Lett. **114**, 143001 (2015).
15. J.-W. Geng, W.-H. Xiong, X.-R. Xiao, L.-Y. Peng, and Q. Gong, "Nonadiabatic electron dynamics in orthogonal two-color laser fields with comparable intensities," Phys. Rev. Lett. **115**, 193001 (2015).
16. X. Xie, T. Wang, S. Yu, X. Lai, S. Roither, D. Kartashov, A. Baltuška, X. Liu, A. Staudte, and M. Kitzler, "Disentangling intracycle interferences in photoelectron momentum distributions using orthogonal two-color laser fields," Phys. Rev. Lett. **119**, 243201 (2017).
17. H. Agueny, "Quantum control of ultrafast ionization with orthogonal two-color laser pulses," unpublished .
18. Y. Zhou, Q. Liao, Q. Zhang, W. Hong, and P. Lu, "Controlling nonsequential double ionization via two-color few-cycle pulses," Opt. Express **18**, 632–638 (2010).
19. Y. Zhou, C. Huang, A. Tong, Q. Liao, and P. Lu, "Correlated electron dynamics in nonsequential double ionization by orthogonal two-color laser pulses," Opt. Express **19**, 2301–2308 (2011).
20. X. Ma, Y. Zhou, Y. Chen, M. Li, Y. Li, Q. Zhang, and P. Lu, "Timing the release of the correlated electrons in strong-field nonsequential double ionization by circularly polarized two-color laser fields," Opt. Express **27**, 1825–1837 (2019).
21. M. Protopapas, D. G. Lappas, and P. L. Knight, "Strong field ionization in arbitrary laser polarizations," Phys. Rev. Lett. **79**, 4550–4553 (1997).
22. L. Zhang, X. Xie, S. Roither, D. Kartashov, Y. Wang, C. Wang, M. Schöffler, D. Shafir, P. B. Corkum, A. Baltuška, I. Ivanov, A. Kheifets, X. Liu, A. Staudte, and M. Kitzler, "Laser-sub-cycle two-dimensional electron-momentum mapping using orthogonal two-color fields," Phys. Rev. A **90**, 061401 (2014).
23. M. Feit, J. Fleck Jr, and A. Steiger, "Solution of the schrödinger equation by a spectral method," J. Comput. Phys. **47**, 412–433 (1982).
24. H. Agueny, A. Makhoute, A. Dubois, and J. P. Hansen, "Coherent electron emission beyond young-type interference from diatomic molecules," Phys. Rev. A **93**, 012713 (2016).
25. H. Agueny and J. P. Hansen, "Quantum multiscattering interferences in collision-induced coherent electron emission from diatomic molecules by swift ion impact," Phys. Rev. A **94**, 052702 (2016).
26. V. Kukulin and V. Pomerantsev, "The orthogonal projection method in scattering theory," Ann. Phys. **111**, 330 – 363 (1978).
27. H. Agueny, A. Makhoute, A. Dubois, I. Ajana, and G. Rahali, "Laser-assisted inelastic scattering of electrons by helium atoms," Phys. Rev. A **92**, 013423 (2015).
28. P. V. Demekhin and L. S. Cederbaum, "ac Stark effect in the electronic continuum and its impact on the photoionization of atoms by coherent intense short high-frequency laser pulses," Phys. Rev. A **88**, 043414 (2013).
29. H. Agueny, A. Makhoute, and A. Dubois, "Dynamic-Stark-effect-induced coherent mixture of virtual paths in laser-dressed helium: energetic electron impact excitation," J. Phys. B: At. Mol. Opt. Phys. **50**, 125002 (2017).
30. The phase of the ground state $\zeta(t)$ is fitted to an arctan function to remove the linearity behavior of this phase, allowing thus to identify the non-linearity of the phase with higher visibility.
31. B. J. Sussman, "Five ways to the nonresonant dynamic Stark effect," Am. J. Phys. **79**, 477–484 (2011).
32. P. V. Demekhin and L. S. Cederbaum, "Dynamic interference of photoelectrons produced by high-frequency laser pulses," Phys. Rev. Lett. **108**, 253001 (2012).
33. H. Agueny and J. P. Hansen, "High-order photoelectron holography in the midinfrared-wavelength regime," Phys. Rev. A **98**, 023414 (2018).